remote sensing

MDPI

Article

Glacier Remote Sensing using Sentinel-2. Part I: Radiometric and Geometric Performance, Application to Ice Velocity, and Comparison to Landsat 8

Andreas Kääb [1,*], Solveig H. Winsvold [1], Bas Altena [1], Christopher Nuth [1], Thomas Nagler [2] and Jan Wuite [2]

[1] Department of Geosciences, University of Oslo, P.O. Box 1047, 0316 Oslo, Norway;
E-Mails: kaaeab@geo.uio.no (A.K); s.h.winsvold@geo.uio.no (S.H.W); bas.altena@geo.uio.no (B.A.); chris.nuth@geo.uio.no (C.N)
[2] ENVEO, Innsbruck, Austria
* Correspondence: kaeaeb@geo.uio.no; Tel.: +47-228-558-12

Academic Editor: name
Received: date; Accepted: date; Published: date

Abstract: With its temporal resolution of 10 days (5 days with two satellites, and significantly more at high latitudes), its swath width of 290 km, and its 10m and 20m-resolution bands from the visible to the shortwave infrared, the European Sentinel-2 satellites have a large potential for glacier remote sensing. Testing Level 1C commissioning and ramp-up phase data, we find a high radiometric performance, however with slight striping effects under certain conditions that will usually not affect typical glacier applications. Through co-registration of repeat Sentinal-2 data we also find lateral offset patterns and offset noise on the order of a few metres, which will also in most cases not complicate glaciological applications. Absolute geolocation of the data investigated was at the time of writing on the order of one pixel. The most severe geometric problem stems from vertical errors of the DEM used for ortho-rectifying Sentinel-2 data. These errors propagate into locally varying lateral offsets in the images, up to several pixels with respect to other georeferenced data, or between Sentinel-2 data from different orbits. Finally, we characterize the potential and limitations of tracking glacier flow from repeat Sentinel-2 data using a set of typical glaciers in different environments: Aletsch Glacier, Swiss Alps; Fox Glacier, New Zealand; Jakobshavn Isbree, Greenland; Antarctic Peninsula at the Larsen C ice shelf.

Keywords: Sentinel-2; Landsat; orthorectification; geolocation; ice velocity; Aletsch Glacier; Fox Glacier, Jakobshavn Isbree, Antarctic Peninsula

1. Introduction

Landsat-type medium-resolution optical satellite sensors are a backbone for operational worldwide glacier mapping and monitoring, and are for instance applied to retrieve glacier outlines, glacier surface facies, or ice velocities [1]. In 2013, Landsat 8 significantly improved the possibilities for glacier observations from space in comparison to Landsat 5 and 7, in particular due to its better radiometric performance (12 bit compared to 8 bit of Landsat 5 and 7; reduced noise level), better geometric stability (pushbroom principle against scanner principle), and significantly higher acquisition rate (i.e. higher temporal resolution) due to advanced onboard recording and ground transmission capabilities [2]. The Copernicus Sentinel-2 satellite series, consisting of 2 satellites A and B, will further enhance the worldwide monitoring of glaciers and land ice masses and their changes. The first of the satellites, Sentinel 2A, was launched in June 2015, followed by the second satellite, Sentinel-2B, planned for launch in 2016. Both Sentinel-2 satellites operate the MultiSpectral Instrument (MSI) with enhanced spectral and geometric capabilities and high repeat observation capabilities.

Among the most important characteristics of MSI for glacier investigations are [3,4]:

- 4 visible and near-infrared (VNIR) bands have 10 m spatial resolution, compared to 30 m (15 m for pan) for Landsat 8 OLI (Figure 1);
- 6 VNIR and short-wave infrared bands (SWIR) have 20 m resolution, compared to 30 m for Landsat 8 OLI;
- Sentinel-2 MSI swath width is 290 km against 185 km of Landsat 8;
- Sentinel-2A orbit repeat rate is 10 days against 16 days of Landsat 8, and will become 5 days from the same relative orbit after the launch of Sentinel-2B. The actual frequency of repeat acquisitions however depends on the capacity of the entire system and acquisition plan. For higher latitudes where the swaths from neighbour orbits overlap, the potential revisit time will also be shorter than 10 or 5 days (Figure 2).
- It should also be noted that Sentinel-2 carries no thermal instrument in contrast to Landsat 8.

Some performance parameters connected to medium-resolution optical satellite sensors are of particular importance for glacier investigations: automated glacier mapping relies often on VNIR/SWIR band ratios where thresholds are typically set manually [1,5-7]. For such scene-specific segmentation, the relative radiometric precision between individual pixels can be more important than the absolute radiometric accuracy and its stability over time. Also ice velocity measurements, which are typically retrieved by correlating repeat observations, are widely insensitive to absolute radiance calibration variations. They are rather affected by radiometric noise or patterns in the data such as stripes, which reduce accuracy or may even lead to mismatches.

Similarly, the relative geometric precision, i.e. how accurate is the relative geo-location of neighbour pixels, is of importance for glacier mapping and velocity measurements as it degrades accuracy [8]. This type of geo-location error is also called co-registration accuracy, or co-location accuracy, as it can be estimated from the residuals after co-registering repeat data over the same area.

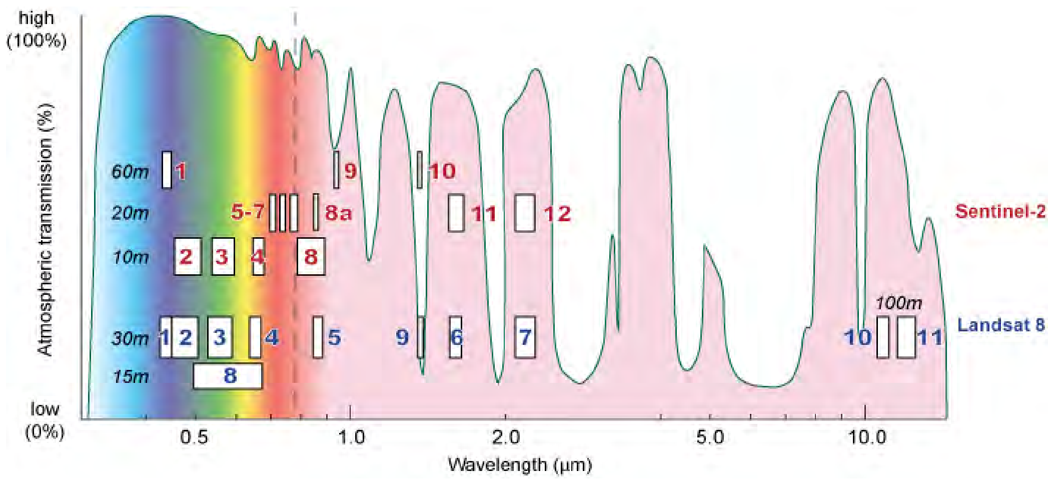

Figure 1. Sentinel-2A bands in comparison to Landsat 8.

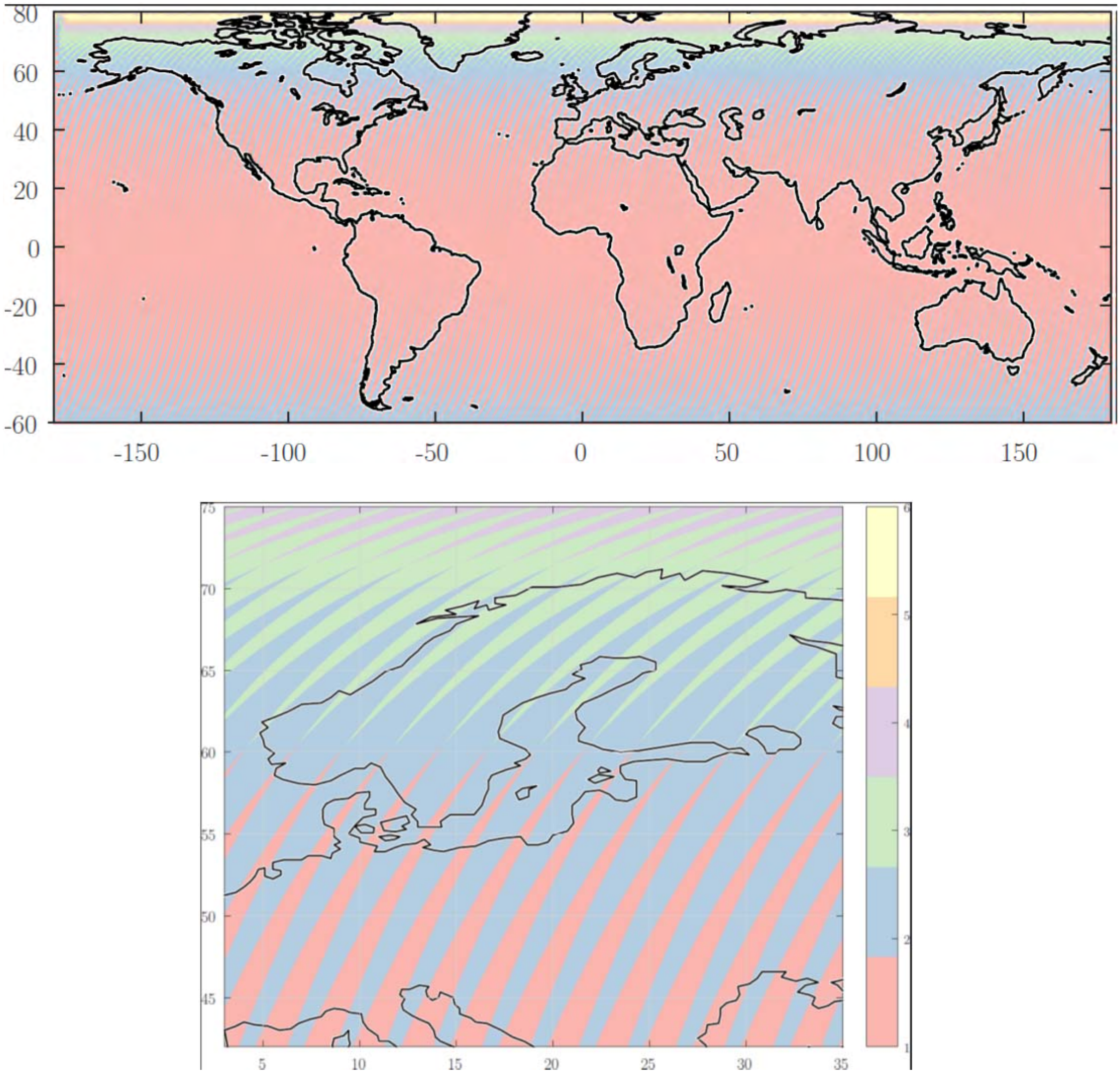

Figure 2. Sentinel-2 swath pattern and colour-coded number of relative orbits from which a point on the ground is seen. Upper panel: global pattern; lower panel: detail over Europe. In the south of Norway, for instance, every ground point is seen from two different relative orbits, in the very north of Norway from three orbits, increasing the temporal resolution of Sentinel-2.

Absolute geo-location errors, i.e. shifts, rotation, scale or higher order deformation of an image with respect to true ground coordinates, misplace measurement results and thus affect comparison to data from other sources or between repeat data [9]. The effect of geo-location biases depends on the application, and will be more problematic for mapping glacier terminus changes, where the signal to be observed is of the same order of magnitude as the potential geolocation error, than for displacement measurement points within low-gradient glacier velocity fields, where velocities are very similar within the range of potential geolocation error.

In part 1 of this study, we investigate the Sentinel-2A radiometric and geometric performance with focus on glaciological applications, and demonstrate ice velocities from Sentinel-2. Part 2 of the study [10] focusses on exploitation of the Sentinel-2 spectral content for mapping of glaciers, glacier facies and other glacier processes. It is important to note that our analyses are based on Sentinel-2A Level 1C data, mainly acquired during ramp-up phase, but also some data from the commissioning phase of the mission. As some image and processing parameters have changed already between both phases (most notably the radiometric scale of the digital numbers provided was increased from 1-1000 to 1-10000) or might further change, we focus on conclusions that should also hold for the operational phase. Level 1C data are orthorectified, similar to Landsat 8 data, using a digital elevation model (DEM).

2. Radiometric noise and patterns

2.1. Performance over homogenous surfaces

Radiometric noise and noise patterns are important quality characteristics of a sensor and may degrade the accuracy of classification results and offset tracking. Here, we investigate these figures from scenes over homogenous surfaces.

Sentinel-2 bands 4, 8 and 11 are likely among the most important bands for glacier mapping and offset tracking. Over dark and calm water without sun glitter, we find along-track stripes of one pixel in width (confirmed in several scenes at different locations) and on the order of ±7 digital numbers (DN) for band 4 (Red, 10 m resolution), ±5 DN for band 8 (NIR, 10 m) and ±4 DN for band 11 (SWIR, 20 m) (Figure 3). (Note, these DN values refer to ramp-up phase data where DNs are scaled from 0 to 10'000). These along-track stripes are likely from imperfect de-striping or detector calibration. We also find stripes of similar magnitude in, roughly, cross-track direction (Figure 3).

For bright surfaces like firn and snow, these patterns are observed suggesting they are related to low radiance levels at the detectors. Occasionally over homogenous bright surfaces, such as Antarctic ice shelves (section 4.4) we find radiometric steps between the 12 pushbroom modules that form the Sentinel-2 focal plane on the order of 30 DN (see below sections 3.1 and 3.2 for geometric offsets between the modules). Most glaciological applications will thus be little affected by this kind of striping, perhaps with the exception of dark shadow areas. The visibility of the marginal stripes suggests a radiometric precision of Sentinel-2 MSI even better than the above DN ranges of approximately 7-4 DNs as these stripe patterns represent systematic errors that could be removed by improved calibration procedures within the processing system or by empirical de-striping by the user.

For medium-bright homogenous surfaces, such as in deserts, we find a random radiometric noise level on the same order as the above stripes (~ ±5 DN), for bright snow and firn areas (accumulation areas) even less. For comparison, noise levels of Landsat 8 DNs are on the order of 30DN for bands 4, 5, 6 and 8 (red, NIR, SWIR, 30 m, and pan, 15m), and thus no stripes are detectable on dark surfaces. Landsat 8 DNs are scaled to 16 bit (65536) so that their noise level translates to similar values as for Sentinel-2.

The effect of the noise described above on band ratios, the most established method for automatic mapping of ice surfaces [10], is on the order of 1%. For instance, the resulting uncertainty of a threshold of 2.0 for typical mapping conditions (th1 in [10]) becomes ± 0.015, which is far below the uncertainty of manually setting and adjusting this threshold, as is usually done. The effect of the above radiometric noise on multispectral analyses and offset tracking seems negligible to us and by far smaller than uncertainties by varying glacier properties and imaging conditions.

Note, that the above values given for both sensors are based on a limited number of locations and scenes, and thus form no systematic investigation and only provide an order of magnitude for radiometric noise. We cannot be sure to what extent real variations of ground reflectance of the tested surfaces contaminate our results, though we tried to visually avoid such effects.

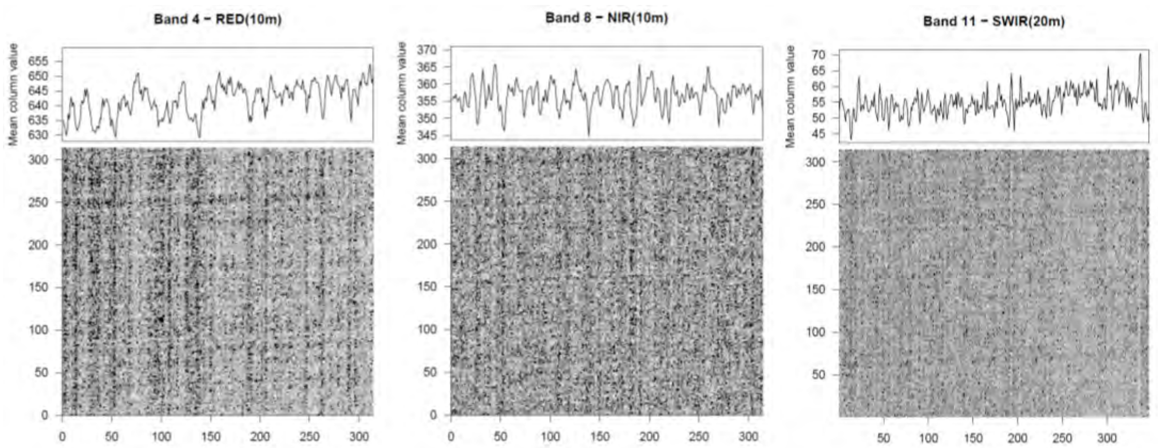

Figure 3. Sections of about 300 by 300 pixels over dark water in Sentinel-2 bands 4, 8 and 11 with enhanced histograms. Both along-track (vertical) and cross-track (horizontal) stripes become visible over such dark surfaces. The upper lines indicate the along-track column means in digital numbers (DN). Stripes amount on average between ±7 DN and ±4 DN for bands 4 and 11, respectively.

2.2. Performance in shadows

Glaciers are often situated in mountains with rugged topography so that the radiometric performance of an optical sensor in mountain or cloud shadow areas is important for achieving maximum coverage of glacier mapping and velocity measurements. Figure 4 shows a deeply shadowed mountain flank seen through Sentinel-2, Landsat 7 and 8. This example, and similar other tests confirm that ground details in shadow areas become well visible through the original 12-bit radiometric resolution of Sentinel-2 MSI (and Landsat 8 OLI), in strong contrast to 8-bit data such as from Landsat 7 ETM+ or ASTER. This improved performance in shadows is important for glacier mapping as it can reduce problems within multispectral classification of ice and snow. In the 12-bit images, offset tracking over glacier sections in cast shadow performs almost as well as outside of the shadows, in contrast to 8-bit images where tracking typically fails completely. Only the shadow boundaries themselves cause problems in the 12-bit data as they represent a dominant contrast feature so that shadow margins are tracked between repeat images, instead of the, typically, weaker glacier surface features.

Similarly to shadow areas, the original 12-bit radiometric resolution of Sentinel-2 (and Landsat 8) data also avoids radiometric saturation over bright snow and firn surfaces, which was a common problem and limiting factor for using 8-bit images over glaciers and snow. The higher radiometric resolution is of great benefit for offset tracking over snow and ice surfaces that else lack visual contrast that could be matched between images. We also foresee that studies on mapping and characterizing ice and snow surfaces will be enhanced by the strongly increased level of radiometric detail, for instance mapping of snow lines or snow/firn/ice properties, albedo changes, or time series analyses [7].

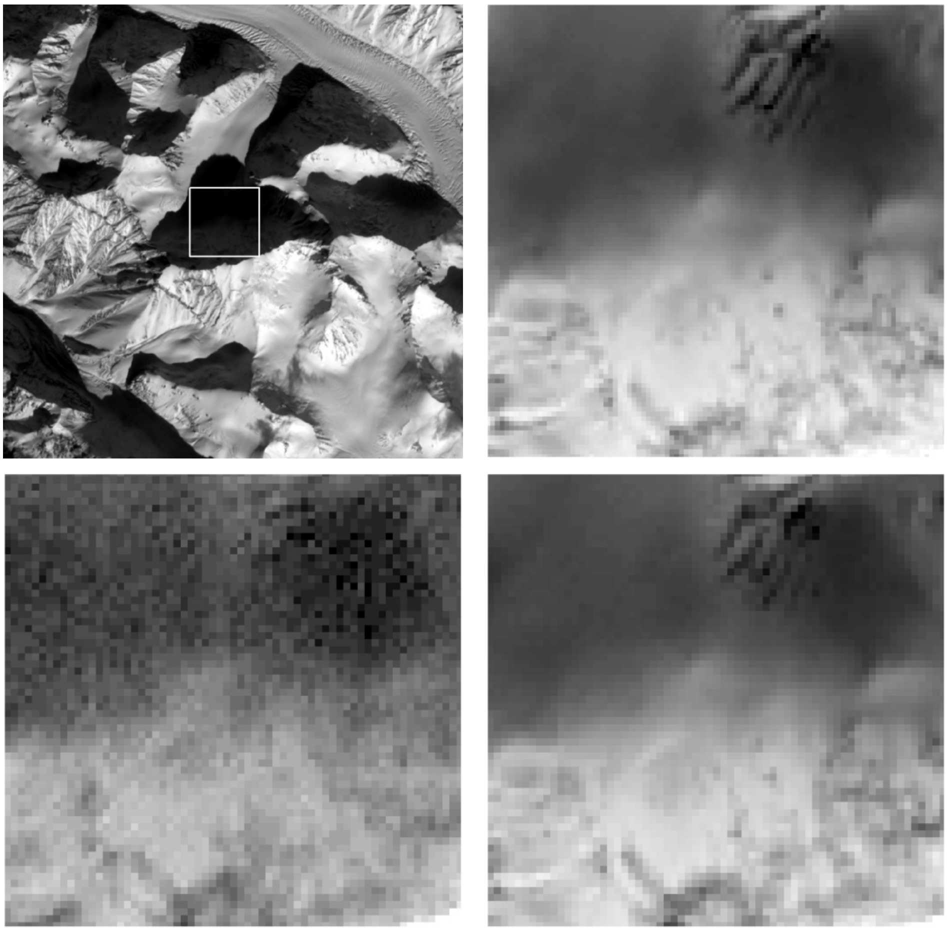

Figure 4. Dark shadow in a mountain flank in the Karakoram. Upper left: overview with location of other panels marked by a white square of 1 × 1 km in size. Upper right: section of a Sentinel-2 image (30 Nov 2015); lower left: Landsat 7 ETM+ (17 Nov 2001); lower right: Landsat 8 (2 Dec 2015). All examples are using band 8 of the respective sensors with enhanced histogram. North to the top. Note the crevasses to the upper middle of the Sentinel-2 and Landsat 8 images.

3. Geometric performance and DEM effects

The geometric performance of Sentinel-2A data in view of glacier applications can be separated into three error-budget terms:

First, the relative geo-locational precision between different data, also called co-registration accuracy. This group of errors can be random (i.e. noise) but also contain systematic patterns such as attitude jitter or calibration errors. (The latter error patterns could also be seen as higher-order components of the following error category).

Second, mainly shifts, but also rotation or deformation, apply to entire scenes and are scene-specific or system-specific geo-location biases in the image data with respect to the true ground location of the measurements. Typically, these biases stem from errors or inaccuracies in spacecraft attitude or position measurements or in the subsequent solution of the image orientation parameters.

Third, and of large practical significance for glacier and high-mountain applications, vertical errors in a DEM elevation used for orthorectification or terrain correction propagate into a pattern of local horizontal off-nadir offsets in the orthorectified products such as Landsat L1T or Sentinel-2 L1C. The effect of these elevation errors depends on the off-nadir view angle, in particular in cross-track direction, and the magnitude of the elevation error (Figure 5). The maximum off-nadir distance of a point in a Sentinel-2 scene can be 145 km so that a vertical DEM error Δh translates in the worst case into a horizontal georeference offset in cross-track direction of

$$d_{max(S2)} \approx \Delta h/5.5 \quad (1)$$

The respective orthorectification offset in a Landsat scene can be up to approximately

$$d_{max(Landsat)} \approx \Delta h/7.5 \quad (2)$$

When comparing two orthoimages from orbits on different sides of a ground point zenith, the above orthorectification offsets in cross-track direction add up. For instance in Figure 5, when comparing an orthoimage from orbit i with one from orbit j, the offset between projections Pi and Pj of ground point P becomes visible. The maximum relative offset Δd between two Sentinel-2 scenes from neighbour orbits can thus be.

$$\Delta d_{max(S2)} \approx \Delta h/2.7 \quad (3)$$

If cross-track offsets of this magnitude appear in practice and need to be accounted for depends much on orbit pattern and latitude, and on the necessity to use data from different orbits instead of only one, i.e. on for instance cloud cover or change rate on the ground. Figure 2 gives an impression of the Sentinel-2 swath pattern and thus the distribution of respective overlaps.

Only the difference of the two individual offsets becomes effective if the two orbits are on the same side with respect to a ground point zenith, e.g. offset Pi - Pk in Figure 5 becomes visible.

Two types of errors contribute to vertical offsets Δh between the terrain and its approximation by a DEM: (a) measurement or production errors where DEM elevation does not agree with terrain elevation at the time of acquisition of the elevation data, and (b) changes in terrain elevation over time between elevation measurement and satellite scene acquisition. For glaciological applications, the most prominent DEM error of type (b) is due to glacier elevation changes, which can amount to many tens or even hundreds of metres depending on the age difference between the DEM and satellite image. It is beyond the scope of this contribution to discuss in detail the DEMs used for orthorectification of Sentinel-2 or Landsat data, but it is clear that type (a) can reach the same order of magnitude as type (b).

The above three horizontal bias categories (overall scene offsets, higher-order offset patterns, orthorectification offsets due to DEM errors) are superimposed in practice but can be isolated partially by special experimental setups.

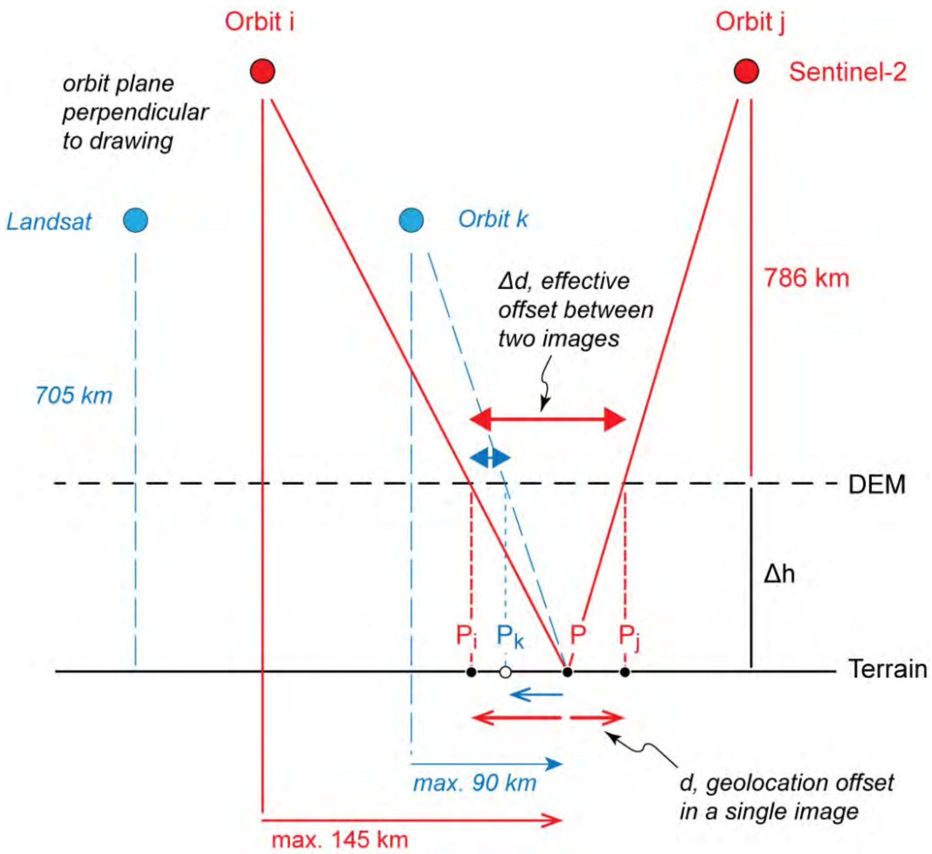

Figure 5. Vertical errors Δh in a DEM used for orthoprojection of satellite scenes translate into horizontal orthoimage offsets from the true location of point P. These cross-track offsets depend on the magnitude of Δh and the off-nadir cross-track look angle of the sensor towards point P. Compared to true ground coordinates of point P the horizontal offsets P-P_i, P-P_j, or P-P_k become effective, while the offsets P_i-P_j, or P_i-P_k appear when comparing two orthoimages from different orbits. View in orbit plane.

3.1. Co-registration of data from repeat orbits

When co-registering two repeat orthoimages taken from the same relative orbit (repeat orbit), DEM effects will be present but have the same pattern in both data sets so that they become mostly eliminated in the offset field obtained from correlating the two images. The final offset field contains thus differential geolocation noise and biases of higher orders such as shifts, jitter etc. For related experiments we choose scenes with good visual contrast for matching and little surface changes expected, conditions often offered by deserts. We use standard normalized cross-correlation to track offsets [11,12].

From tests based on repeat Sentinel-2 commissioning and ramp-up phase data (band 8, NIR) over the Sahara and over the border region between Afghanistan and Iran we find mean offsets, i.e. biases, on the order of 1-3 m in each cross-track and along-track direction, in some cases up to 10 m in along-track direction. The standard deviations of these mean biases, i.e. the random component of co-registration, is on the order of ±1-2 m. Some of the co-registration tests reveal offset patterns, both in along- and cross-track directions; mostly misalignments at the overlaps of the 12 adjacent pushbroom modules that cover the 290 km swath of Sentinel-2 (Figure 6), and more seldom jitter undulations (vibrations in attitude angles) of some 7-8 km wavelength and an amplitude on the order of 1 m (Figure 7). It should be noted that offset patterns visible in co-registration represent the sum of two individual patterns, the one from the first and the other from the second image. The superposition of the two wave patterns can be destructive or constructive, for instance even if present in both scenes co-registered it can be cancelled out in the offsets between both scenes, or be exaggerated (doubled in maximum).

In sum, the co-registration accuracy found for the Sentinel-2 data investigated is on the order of 1/10 of a 10 m pixel. Typically, such precision is also believed to be close to the matching accuracy achievable so that parts of this estimate could actually be due to matching inaccuracies rather than Sentinel-2 geolocation noise. In order to better quantify and characterise the biases and offset patterns found, a systematic and dedicated study with significantly more data over more test sites would be necessary. Seen positively, the detectability of the patterns described above, and with that the potential to correct for it, points towards Sentinel-2 data having a potential relative geometric precision exceeding 1/10 of a pixel as estimated here for the 10m band 8. Co-registration of 20m-bands was not investigated here, but if the same findings hold as for band 8, the ±1-2 m precision found here translates to almost 1/20 of a pixel for 20m-bands.

To our best knowledge, it is planned to register in future Sentinel-2 processor versions new scenes to a reference scene from the same relative orbit. This measure would largely remove the above co-registration biases, but could also remove parts of the higher-order offset patterns seen, depending on the co-registration model applied.

For reference, we also performed similar co-registration studies for band 8 (pan, 15m) of Landsat 7 ETM+ and Landsat 8 (Figure 8). From several scenes over the Kelso area in California we found for Landsat 7 mean co-registration biases of around 1 – 1.5m with a standard deviation of ±3 – 4 m, both in along- and cross-track directions, and biases of 1 m with a standard deviation of ±2.5 – 3m for Landsat 8. Strong cross-track undulations where found for Landsat 7, presumably resulting from a kind of jitter related to the scanner principle of this instrument against the pushbroom principle used for Landsat 8 and Sentinel-2.

Again and as for all tests presented in section 3, the sample size behind this assessment is limited and does not necessarily reflect an average performance of Landsat 7 and 8. We also would like to stress that most tests areas within section 3 are situated in mid to low latitudes and that the offset patterns found are thus not necessary fully representative for high latitudes, for instance due to the different orbit azimuth with respect to the Earth's rotation axis.

As a side-note, we find in many of the coregistration patterns investigated over arid landscapes (Sahara, Iran, Australia) also patterns that match natural surface patterns, in particular in the cross-track offsets (for instance, Figure 7, right panel, blue offset area to the top middle). As our impression is that these offsets of up to several metres are especially found over dry sandy areas, and for instance not over bedrock, we speculate that these offset patterns could stem from small vertical offsets Δh in the SRTM elevation model directly due to penetration of radar waves into the sandy dry soil (RefXXX) or due to local SRTM DEM shifts due to this penetration. Even if the data compared are from the same relative orbit, small differences in viewing directions could cause small-baseline stereo effects leading to horizontal offsets, Δd, as described in section 3. Such small-angle stereo effects are also involved in the process of focusing the different bands and pushbroom modules onto the ground. Note that only offset differences, Δd, between both scenes coregistered become visible (Figure 5). Also, we cannot completely rule out terrain movements between the two acquisitions such as from dune migration [13,14] or shadow movements, though visual image inspection does in general not support these possibilities.

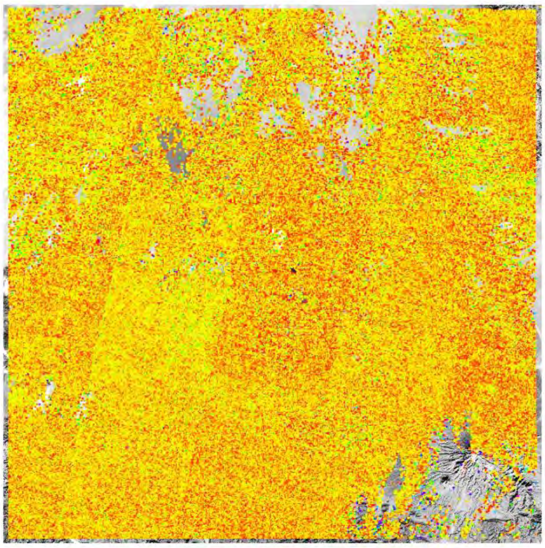

Figure 6. Along-track component of co-registration offsets between Sentinel-2 data from the same orbit, R120, from 28.11.2015 and 8.12.2015. UTM-tile T40RGS, 110x110 km in size. North is to the top and the five slightly oblique blocks of about 20 km width indicate the orbit direction from north to south. There is an overall shift between the two scenes of about 8.5 m, and offsets between the pushbroom modules are up to about 1-2 m.

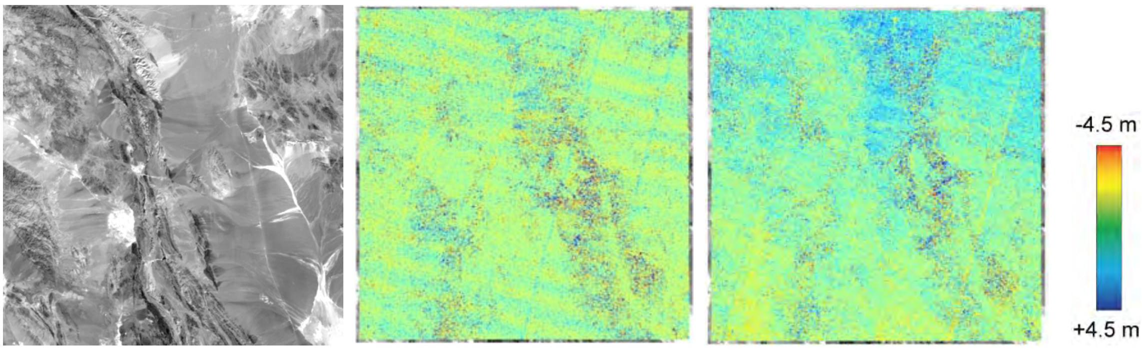

Figure 7. Along-track component (middle panel) and cross-track component (right panel) of coregistration offsets between Sentinel-2 data from the same orbit, R120, from 30.8.2015 and 9.9.2015 (commissioning phase), showing jitter. Complete UTM-tile T41SKS, border region between Iran and Afghanistan.

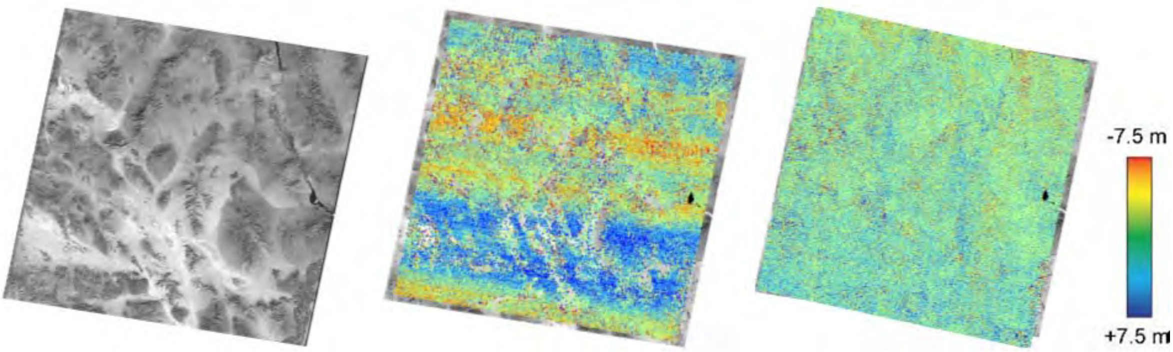

Figure 8. Cross-track components of Landsat coregistrations. Path/row 39/36. Middle panel: Landsat 7 band 8 data of day 337 and 353 of 2002, right panel Landsat 8 band 8 data day 359 of 2013 and day 10 of 2014.

3.2. Co-registration of data from neighbouring orbits

When co-registering repeat data sets from neighbour orbits, the vector sum of two horizontal projections of vertical DEM errors becomes visible in addition to the relative and absolute geolocation errors described in the above section. DEM errors and thus their horizontal propagation into orthorectified data are expected to be particularly large for mountain areas with their steep slopes or where the DEM source data are of reduced accuracy in general. As a special case over glaciers, DEM elevations are almost by necessity outdated with respect to the time of image acquisition, unless simultaneous stereo data are available (e.g. for ASTER or SPOT5). The elevation errors will typically be largest at the glacier termini. When using repeat data over glaciers the detection of DEM errors is complicated by the fact that ice motion vectors are superimposed over the DEM error projections (see section 4.1), unless ice motion is negligible over the observation period.

The DEM currently used for orthorectification of Sentinel-2 is to our best knowledge the PlanetDEM 90 (http://www.planetobserver.com), which is "… a multi-source elevation product processed from SRTM data (Shuttle Radar Topography Mission) version 4.1, corrected and completed with many other source data (cartographic, etc.)".

For a test in Northern Norway, i.e. outside of the SRTM coverage, we difference the topographic DEM by the Norwegian mapping agency (Statens kartverk) and the DEM from www.viewfinderpanoramas.org, which is based on Soviet Union cartographic maps. Figure 9, left panel, shows vertical differences that reach typically many tens of metres, up to 100-200 m in a number of places. We then calculate the horizontal offsets between Sentinel-2 scenes acquired on 18.8. and 22.8.2015 during the relative orbits R051 and R008, respectively. The test area lies between the two ground-projected orbit tracks, roughly 45 km way from each of them in both directions. I.e., the orbit tracks have a cross-track distance of about 90 km from each other (case Pi-Pj in Figure 5). For each of the two images vertical DEM errors propagate thus into horizontal offsets d with a ratio of about $\Delta h/18$, and the total effective offset between the two images Δd becomes $\Delta h/9$. If we scale the horizontal offsets measured between the two Sentinel-2 scenes with this factor we reconstruct the elevation errors Δh that correspond to the horizontal offset field (Figure 9 right). In fact, the reconstructed Δh appears very similar to the actual Δh of the DEM by www.viewfinderpanoramas.org, suggesting that this DEM was in some way incorporated into the DEM used for Sentinel-2 orthorectification, at least over the study area. Based on comparisons with reference data, for instance from national topographic DEMs, we can thus analyse the accuracy and characteristics of the DEM behind Sentinel-2 where based on Soviet maps, or www.viewfinderpanoramas.org, respectively. In this test case, the study area is close to the orbit tracks (45 km). At the image margins (i.e. 145 km off-nadir), elevation errors of 100-200 m would translate into georeference offsets d_{max} of 18-37 m in one scene, and of up to 37-74 m between scenes from different orbits (Δd_{max}, Equation 1).

Similar tests performed with Landsat 8 scenes with cross orbits of ~50km do not show similarity with the elevation differences of Figure 9 and reconstructed DEM errors of up to ~50-60 m imply the use of a more accurate DEM than used for Sentinel-2.

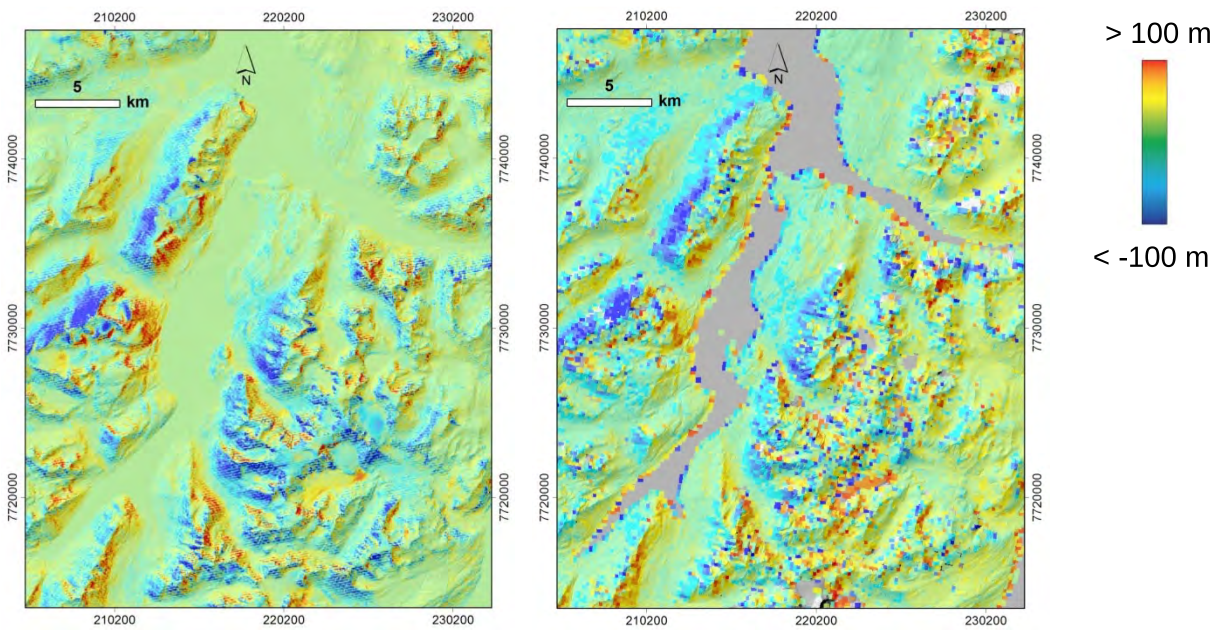

Figure 9. Left: elevation differences between a DEM from the Norwegian mapping agency and a DEM from www.viewfinderpanoramas.org based on Soviet maps. Right: cross-track offsets between two Sentinel-2 scenes of 18.8. and 22.8.2015, UTM-tile T33WXT, Lyngen, Northern Norway. The cross-track offsets (right) are scaled to reconstruct the DEM errors that lead to them. The pattern of both panels is similar, besides typical matching errors. Coordinate grid: UTM zone 35N.

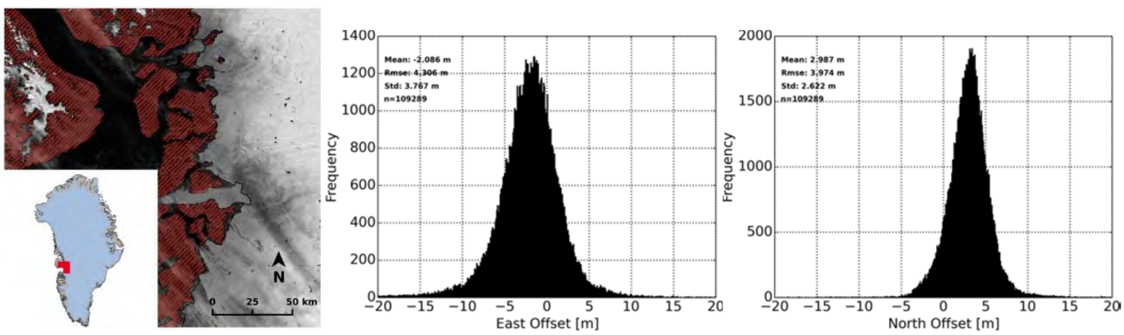

(a) (b) (c)

Figure 10. (a) Map of stable areas (red) in West Greenland near Jacobshavn Isbree used for calculating co-registration accuracy; background image: Sentinel-2, band 8, 16 August 2015. **(b)** and **(c)** histograms of colocation accuracy in Easting and Northing of Sentinel-2 band 8. For coordinates see Figure 15.

For a further test to investigate the co-registration of Sentinel-2 L1C data from overlapping neighbouring orbits, we select ice free areas at the West coast of Greenland and measure offsets by cross-correlation. Moving areas like glaciers, ice sheet and the ocean were masked out using the Randolph Glacier Inventory Version 5.0 [15] and the GIMP ice and ocean mask [16]. The two data sets of relative orbit R68 and R111 were acquired on 16 August and 9 September 2015 (Figure 10). The histograms of displacements for stable terrain indicate a mean mis-location of -2.1 m and +3 m and a standard deviation of 3.8 m and 2.6 m in Easting and Northing direction, respectively, corresponding to 0.2 and 0.3 pixels of band 8. The spreading of the histogram is mostly caused by DEM errors propagating into the orthorectfication of the images from different orbit tracks. Note that due to orbit azimuth, cross-track offsets from DEM errors propagate both into Easting and Northing direction, though predominantly into Easting at the latitude of this test area.

Within the coverage of SRTM vertical DEM errors are expected to be in general smaller than outside SRTM, with however larger errors over steep and glacierised mountains, where SRTM voids are common (see section 3.3). (At this point, we do not know how SRTM voids are treated in the PlanetDEM 90). As a result, cross-track offsets between Sentinel-2 data from different orbits over gentle terrain within SRTM coverage are substantially smaller than the offsets found for instance over Northern Norway. As terrain effects become small, other effects become better visible. Over several test sites over flat desert environments at mid and low latitudes we find cross-track offset patterns similar to the ones in Figure 11 (or offsets in Easting, which is a direction very similar to the cross-track direction). The overlay of the cross-track offsets between different pushbroom modules from both individual overlapping scenes can be destructive, or as seems to be the case here, constructive with offsets between along-track stripes of 5 m or more. In Figure 11, there seems also to be a slight along-track tilt between both scenes. Also, as in the uppermost section of the figure, we find sometimes abrupt east-west steps in the offsets, presumably from steps in the DEM used for orthorectification, or from processor artefacts. For the offsets in Figure 11, we find a mean cross-track offset of 0.7 ± 1.7 m, and an along-track offset of 21 ± 1.7 m (not shown).

Similar tests at the same sites were performed for the overlaps of Landsat 8 scenes taken from neighbouring orbits. We obtain cross-track offsets of around 1 ± 3 m, and along-track offsets of around 1.5 ± 2.5 m. Also for Landsat 8 some along track tilt, and some along-track stripes from the individual push-broom modules become visible, on the order of 3 m and with less clear boundaries than for Sentinel 2 MSI.

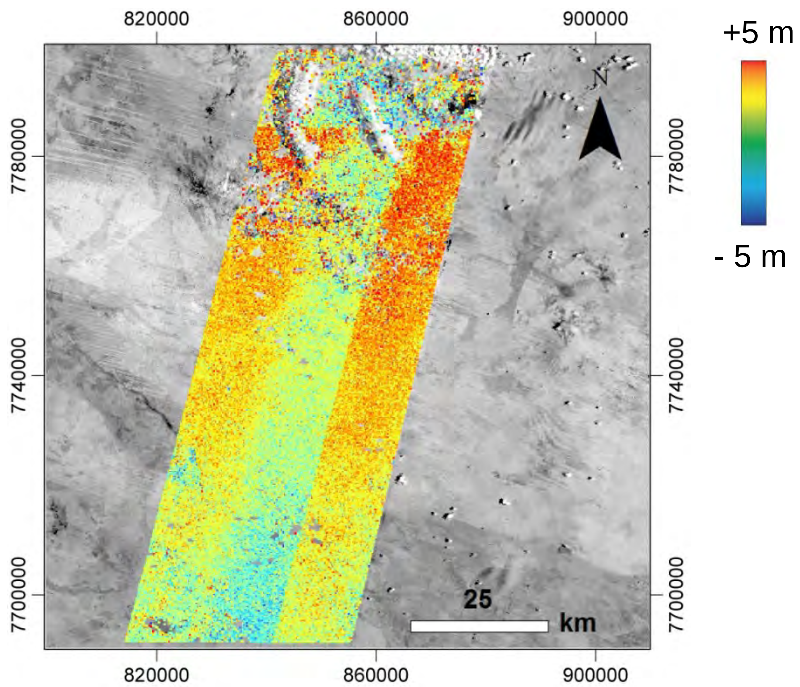

Figure 11. Sentinel-2 cross-track offsets between two neighbouring swaths. Scenes of 29.11 (orbit R131) and 6.12.2015 (R088), UTM-tile T52KHU, Northern Territory, Australia. Coordinates in UTM zone 52.

3.3 Co-registration between Sentinel-2A and Landsat 8 data

As Sentinel-2A and Landsat 8 orbits are not equivalent, comparison of images from both satellites resembles the analysis done in the previous section, with some differences though. Mainly, the geometric setting between the Sentinel-2A and Landsat 8 orbits is different and the orthorectification of data from both systems involves different DEMs, so that the expected offsets between repeat data from Sentinel-2A and Landsat 8 are different to offsets in data from neighbour Sentinel-2 orbits. As Sentinel-2 and Landsat 8 data will be most likely combined in many glacier remote sensing studies, this offset experiment is of as high practical relevance as the comparison for Sentinel-2 data from neighbour orbits. Over glaciers, the analysis of offsets between Sentinel-2 and Landsat 8 can be facilitated by the fact that acquisitions of the same day can be found so that the ice movement component in the offsets becomes negligible for most glaciers.

For such a case of near-simultaneous Landsat 8 and Sentinel-2 acquisitions (8 Sept 2015 over the Swiss Alps, acquisitions ~20 min apart) we match offsets (Figure 12). Maximum cross-track offsets of 20-30 m appear over the glacier tongues (rather 20 m in areas with good matching conditions), but also other parts of the glaciers become distinct in the offset field. The test site lies between the Landsat 8 and Sentinel-2 orbit ground tracks with cross-track distances from image nadir of 80 and -65 km, respectively. In case the Landsat 8 and Sentinel-2 data used were rectified using the same DEM (SRTM?) horizontal offsets d in both images would sum up to $\Delta d = \Delta h/5$, so that the offsets measured correspond to DEM errors of 100 m (perhaps up to 150 m). Elevation losses on this order between the 2000 SRTM DEM and 2015 are completely realistic [17]. Outside of the glaciers, offsets are on the order of a few metres and show also some geographic patterns, likely due to systematic vertical errors of the DEMs used for orthorectification, for instance over forest or steep terrain.

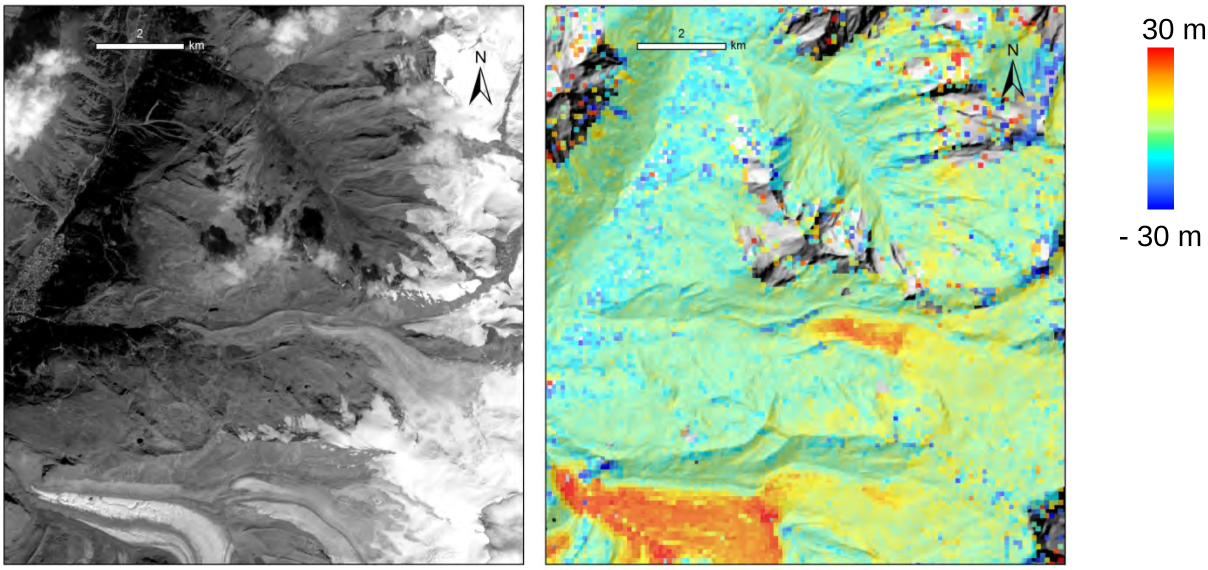

Figure 12. Cross-track offsets (right) between sections of a Landsat 8 and a Sentinel-2 (left) scene of 08 Sept 2015 (10:10 and 10:30 UTC, respectively) over Zermatt, Gorner Glacier and Findelen Glacier, Swiss Alps. Data voids in the offset field are due to mismatches over clouds. Colour-coded offsets underlain by a DEM hillshade. Distinct offsets over the glaciers are due to glacier thickness loss between the date of the DEM used for orthorectification (SRTM of 2000?) and the image acquisition in 2015.

3.4 Co-registration to reference images

A final experiment to test the relative and absolute geolocation accuracy of Sentinel-2 data is their correlation with reference images. Here, we track offsets between the Sentinel-2 tile T32TMS of 29 August 2015, or the Landsat path 195 row 28 image of 30 August 2015, respectively, and the Swiss swissimage25, which is a 25m version of a national airborne orthophoto based on airphotos of 2009-2011. For the Sentinel data, we obtain a mean Easting offset of 12 ± 8 m, and -24 ± 7 m in Northing, for the Landsat data 13 ± 9 m in Easting, and -2 ± 7 m in Northing. The offsets for Landsat are hardly significant, also due to the reduced reference resolution of 25 m and the time span between both data sets that in particular impacts matches in the mountains due to snow cover variations. The Northing offset for the Sentinel-2 tile is roughly in line with occasional along-track offsets of 10 m or more suggested by above tests (section 3.1).

4. Ice velocity measurement

The high spatial resolution of up to 10 m together with the high repeat rate between 10 and a few days, depending on latitude, make Sentinel-2A and then later also Sentinel-2B very suitable for worldwide measurement of glacier motion, both alone and in combination with Landsat 8. Ice dynamics is together with the climatically-driven surface mass balance the key process forming glaciers and therefor a crucial glacier and climate variable [1]. Changes in ice flow can be responsible for large and fast glacier mass changes, for instance when ice flux through a calving front significantly exceeds the accumulation flux into a glacier, or when flow instabilities transfer untypical large ice masses from accumulation or low-ablation zones to ones with high ablation [18]. Glacier surges can pose a hazard by inundating infrastructure or damming up rivers [19]. But also less spectacular changes in glacier dynamics are important to understand, for instance, the conditions and potential reaction of glaciers to climatic changes [20].

Here, we use standard cross-correlation techniques between repeat Sentinel-2A and Landsat data to track the offsets of visual features over time [11,12,21,22]. The purpose thereby is not to develop algorithms that are specialized for Sentinel-2A data but rather to exploit the general potential of these data for ice velocity measurement, among others compared to or in combination with Landsat data.

4.1. European Alps

For Aletsch Glacier, Swiss Alps, we track displacements from Sentinel-2 band 8 data of 30 July and 8 September 2015, i.e. over 40 days, from the same relative orbit R108 (Figure 13, left). Speeds measured range up to 0.8 m/day in an icefall from the Ewigschneefeld glacier. Velocities tracked over 7 August – 8 September (32 days; both images path 194 row 28) from repeat Landsat 8 band 8 data are shown in Figure 13, middle panel. In most parts of the glaciers the Sentinel-2 derived velocity field seems more complete and with less outliers. Visual inspection suggests that this is due to the higher resolution of Sentinel-2 that is able to depict finer details than Landsat 8 so that the image cross-correlation is more successful. The reduced success of Sentinel-2 offsets in the Ewigschneefeld ice fall to the upper middle of Figure 13 compared to Landsat 8 offsets is likely due to marked melt of snow patches between 30 July and 7 August. Also the use of different spectral bands in our comparison might influence matching differences (Sentinel-2: NIR band 8; Landsat 8: VIS pan band 8; [23,24]). The velocities obtained are well in line with other measurements [25,26].

For comparison we also tracked displacements between the Landsat data of 7 August and Sentinel-2 data of 8 September. As the two images are not acquired from the same orbit but are rather taken with off-nadir distances of -80 km and 65 km from the Landsat 8 and Sentinel-2 ground tracks, respectively, effective offsets Δd between both scenes due to DEM errors become $\Delta h/5$. Consequently the cross-track offset components Δd from DEM errors on the Aletsch Glacier dominate the velocity field, so that the cross-track offsets (roughly in east-west direction; E-W) sum up with the ice flow vectors (roughly N-S) to NE-SW vectors (Figure 13, right). Besides this effect, ice velocity tracking between the 7 August Landsat and 8 September Sentinel scenes seems to provide slightly more successful matches than the tracking between Landsat only between 7 August and 9 September In this example, combination between Landsat and Sentinel-2 data for ice velocity measurements could thus be beneficial, while errors in the DEMs used for orthorectification of the data make the results confounding and misleading.

Velocity vectors between the repeat data from same orbits (Figure 13, left and middle panels) are not affected by orthorectification offsets, but the geolocation of the measurements is actually offset by values d, i.e. up to some tens of meters depending on the DEM errors Δh and the off-nadir distance of the locations. This effect will typically not be visible and affect results little, but it might be necessary to observe it for special analyses, for instance velocity change detection, and due to the fact that the offsets d will often vary systematically over a glacier with elevation errors Δh increasing from the accumulation areas towards the glacier tongues (Figure 12).

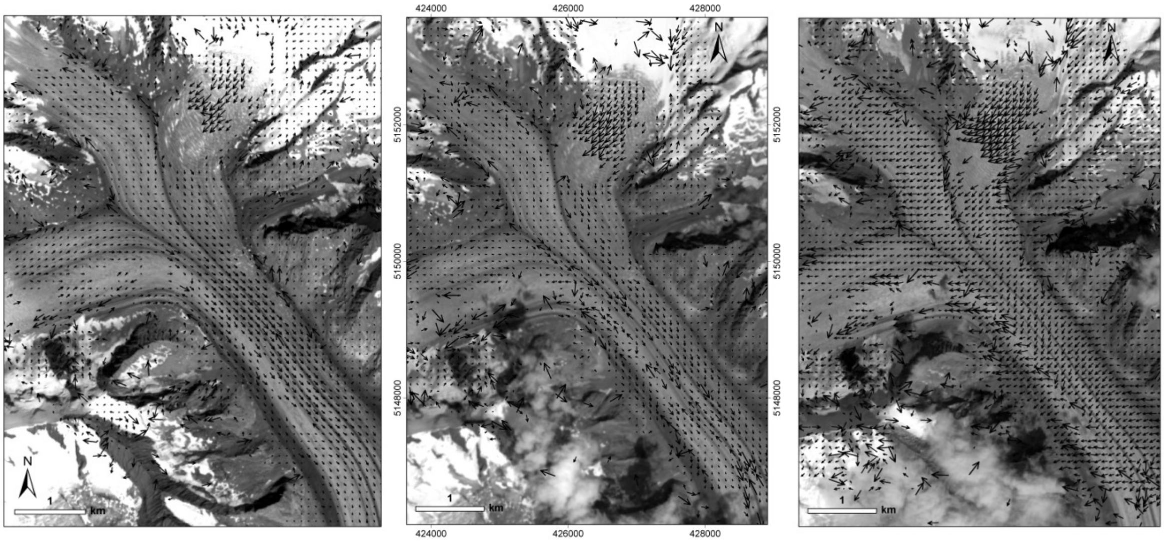

Figure 13. Left: ice velocities between Sentinel-2 data of 30 July (background) and 8 September 2015. Middle: ice velocities between Landsat 8 data of 7 August (background) and 8 September 2015. Right: velocities between Landsat 8 data of 7 August and Sentinel-2 data of 9 September (background). The same matching windows (in ground size) and the same threshold for correlation coefficients have been used. Outliers have not been filtered manually. Coordinates: UTM zone 32N.

4.2. New Zealand

In order to test the performance of Sentinel-2 derived ice velocities over a fast-flowing, maritime (and thus sensitive) alpine glacier, we track displacements over Fox Glacier, New Zealand [27,28] from Sentinel-2 data of 24. Dec 2015, 3. Jan 2016, and 13 Jan 2016 (Figure 14). Displacements were measured in all three combinations, i.e. two subsequent 10-day periods and the full 20-day period, and the residual $\vec{\varepsilon}$ of the vector sum triangulated:

$$\vec{\varepsilon} = \vec{d}_{12} + \vec{d}_{23} - \vec{d}_{13} \ , \quad (4)$$

where $\vec{d} = (dx, dy)$ is the two-dimensional horizontal displacement vector between times 1 and 2, 2 and 3, and 1 and 3, respectively. The residuals of the vector sum were threshold to mask out potential outliers, in combination with low correlation coefficients. Both these residuals and low correlation coefficients exhibit a similar pattern and turn out useful to mask out most erroneous measurements automatically (Figure 14). The large majority of the residuals are 1-2 m in length ($|\varepsilon| = \sqrt{\varepsilon_x^2 + \varepsilon_y^2}$). This number shows that over few repeat orbits, i.e. short times that limit glacier surface changes, ice displacements from Sentinel-2 can be measured with an accuracy of 10-20% of a 10-m pixel even over fast flowing and fast changing medium-size maritime glaciers.

Figure 14 shows the ice speeds on Fox Glacier over 24. Dec – 3. Jan revealing two strong ice streams from the accumulation area, and one weaker one to the south that coalesce and reach maximum speeds of 4.5 m/day below the main ice fall of Fox glacier (see also [28]). Significant speed increases between the two subsequent 10-day periods of up to 1 m/day over 10 days were observed, corresponding to an increase in speed of up to 20%. Most of this increase seems to have happened on the middle, main ice stream (Figure 14, lower panel). These results demonstrate how the high accuracy of the displacements, as suggested based on the triangulated vector-sum residuals, can be applied to quantify ice velocity changes even over short time intervals of days or few weeks.

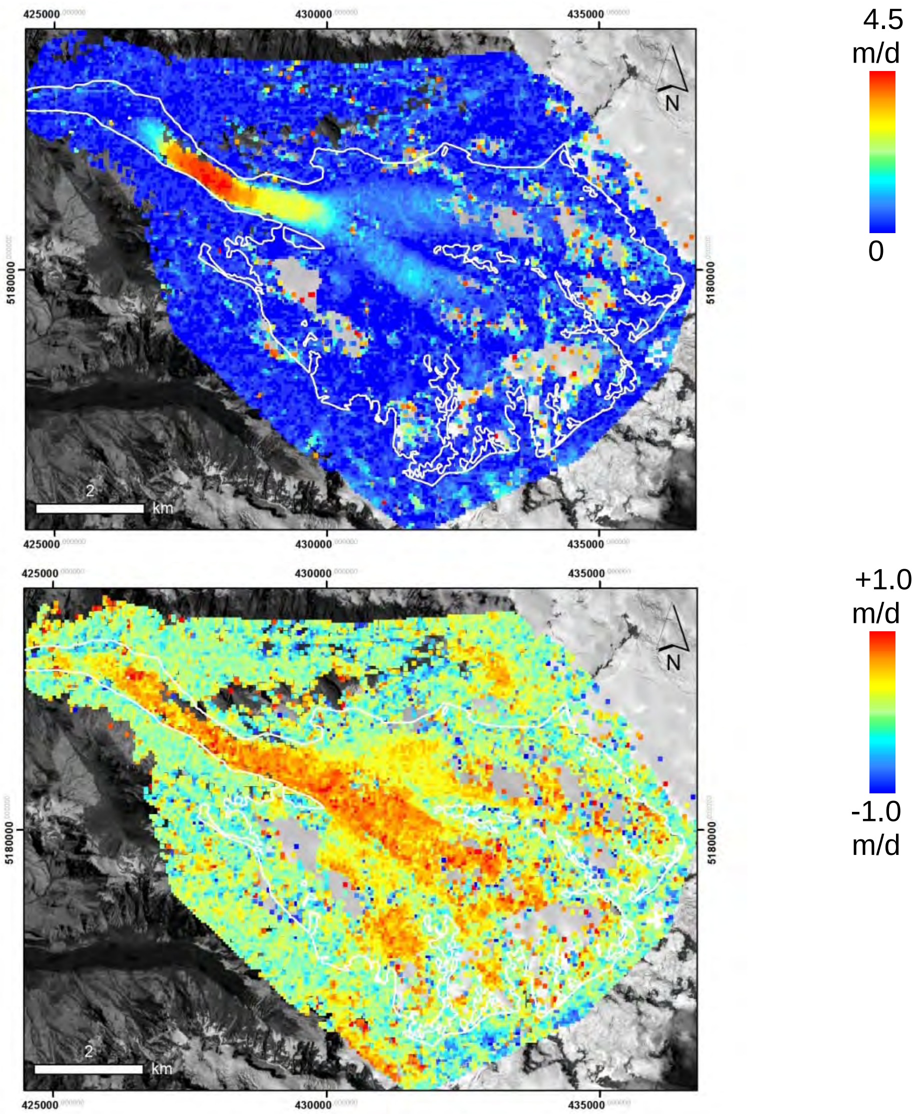

Figure 14. Upper panel: ice speeds on Fox Glacier, New Zealand, from Sentinel-2 data of 24 Dec 2015 and 3 Jan 2016. Lower panel: speed differences between speeds over 24 Dec 2015 – 3 Jan 2016 and 3 Jan 2016 – 13 Jan 2016. Outliers have been removed based on low correlation values and residuals of the vector sum of the two 10-day displacements and the full 20-day displacements. White glacier outlines from [29]. Coordinates in UTM zone 59S.

4.3. Greenland

Figure 15 shows the ice velocity field for the region around Jacobshavn Glacier, West coast of Greenland, using Sentinel-2 data sets of a 23-day interval acquired on 16 August and 8 September 2015. We removed the overall colocation error derived from stable targets by applying a constant offset of 2.1 m and -3.0 m in North and East direction, which corresponds to a velocity of 0.09 m/d and -0.13 m/d for the time interval used. Figure 15b shows the colocation of the adjusted images derived from the stable terrain at the coast (see also Figure 10).

For estimating ice velocity we applied offset tracking with a filter window size of 72 x 72 pixel. Despite the time interval of 23 days and melting conditions on the outlet glaciers and the percolation zone of the ice sheet, the matching procedure detected sufficient features like crevasses and surface melt lakes for generating an almost complete ice velocity field. Some gaps of the ice velocity maps are found in the upper part of the percolation zone and on the terminus of the Jakobshavn Glacier with very high velocities of more than 30 m/d, which requires shorter time periods when surface features are better preserved. In addition, ice flows in a curve which leads to rotation of the features tracked and thus to lack of correlation based on image translation only [30].

We compared the Sentinel-2 ice velocity map with the Greenland mean ice velocity mosaic of 2015 derived from Sentinel-1 Interferometric Wide Swath data [31]. Figure 16 shows velocity profiles along the central flow line for the two outlet glaciers Sermeq Kujalleq (profile 1) and Sermeq Avannarleq (profile 2). We found good agreement between the ice speed from Sentinel-2 and the mean Sentinel-1 based ice velocity map. This agreement points to the possibility of a synergistic use of optical Sentinel-2 and SAR based Sentinel-1 velocity maps for generation of an ice sheet wide velocity map and for monitoring short term temporal variation of ice speed using data from both sensors.

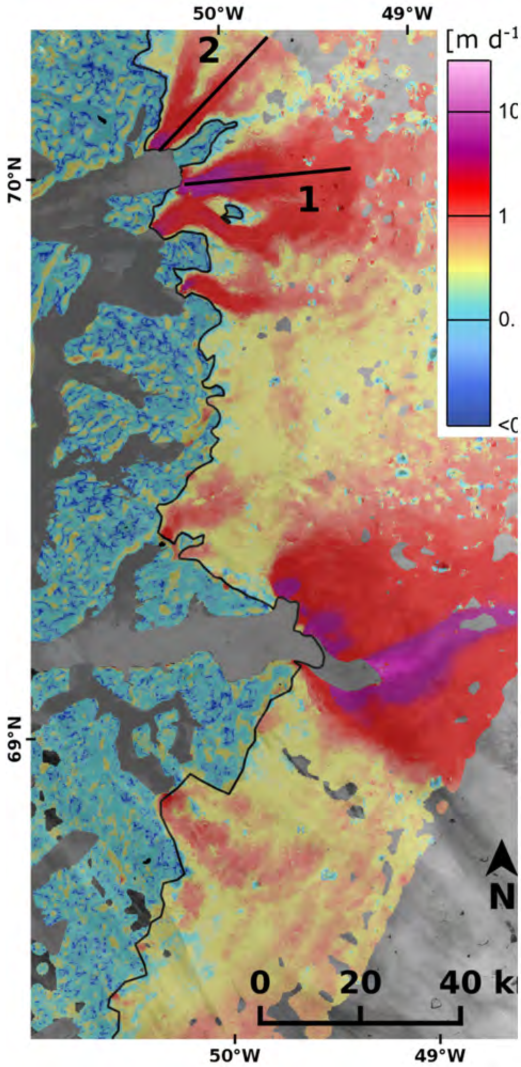

(a)

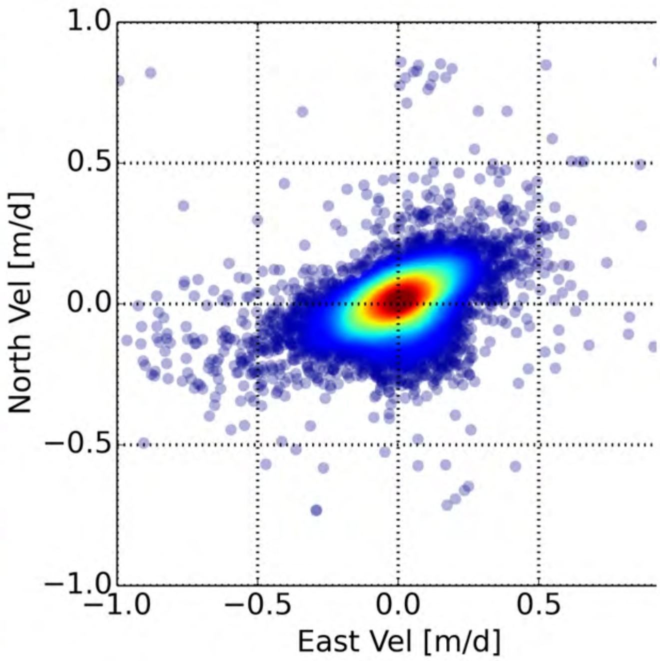

(b)

Figure 15. Sentinel-2 based ice velocity map at West coast of Greenland. Black lines (1) and (2) indicate the velocity profiles, shown in Figure 16. **(b)** frequency-scatterplot of velocity in east and north direction for non-moving areas after adjustment by a constant colocation offset (colour code: from blue to red indicates higher frequency).

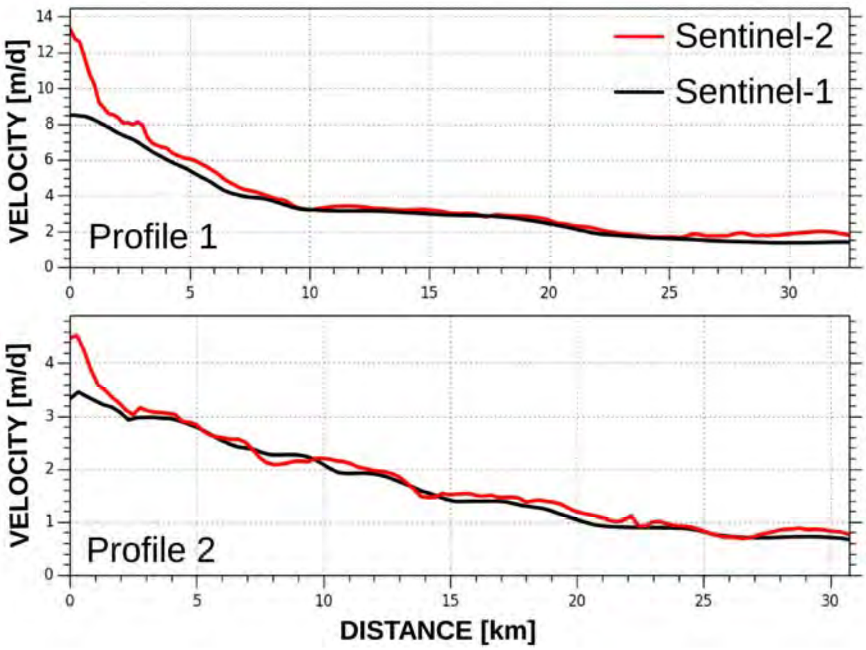

Figure 16. Intercomparison of ice speed along central flowlines of the glaciers Sermeq Kujalleq (profile 1) and Sermeq Avannarleq (profile 2) from Sentinel-2 data from 16 August and 8 September 2015 and the mean Sentinel-1 based ice velocity map [31].

4.4 Antarctic Peninsula

As further test and in strong contrast to the mountain glaciers investigated above, we examine Sentinel-2 derived ice displacements over a section of the Antarctic Peninsula, containing ice plateaus, outlet glaciers, calving glaciers, and parts of the Larsen C ice shelf. Based on Sentinel-2 band 8 images from 8 and 18 January 2016 we obtain maximum speeds of around 6 m/d (Figure 17). Also displacements on sea ice can be resolved (middle left edge of the section, around 2560000 / 600000). The glaciers and parts of the Larsen C ice shelf with surface speeds on the order of 1 m/d (i.e. movements of one Sentinel-2 band 8 pixel and less) become well visible (see also [32]).

We find three types of conditions where the offset tracking failed, as expressed for instance by low correlation values that were then masked out in Figure 17: (i) clouds, as indicated in Figure 17. Near-surface clouds to the lower right corner in the 18 January 2016 image section were not detected by our simple automated cloud detection, but corrupted displacement measurements. (ii) In particular on parts of the plateau lack of coherent visual contrast led to correlation failure. (iii) On large parts of the ice shelf even the matching window size of 40 × 40 pixels (400 × 400 m) used was too small with respect to the typical size of visual features to enable unique identification of corresponding features. In fact, window sizes of 2 × 2 km reveal better results (small panels in Figure 17), and larger windows even better ones (cf. [32]).

The results of Figure 17 were obtained after co-registering the two images over rock outcrops and removing a colocation offset of around -7 m in Easting and 8 m in Northing. Only at few places biases as described in section 3.1 become visible; stripes in along-track direction can be seen at around 2570000/660000 and 2590000/620000 in Figure 17. This confirms the high potential of repeat-orbit Sentinel-2 data for precise ice-velocity measurements even over short time intervals. Biases between the swaths of individual pushbroom modules become visible, and might have to be observed or corrected in special cases, but will in general not have a major effect on ice displacements from Sentinel-2 data.

Only one cloud-free Landsat 8 repeat scene is available for December 2015 and January 2016, so that no comparison to Sentinel-2 velocities was performed. We assume however that Landsat 8 derived velocities over the study site would be similar to Sentinel-2 as the higher spatial resolution of the latter should not be of much advantage given the large window sizes necessary for image matching.

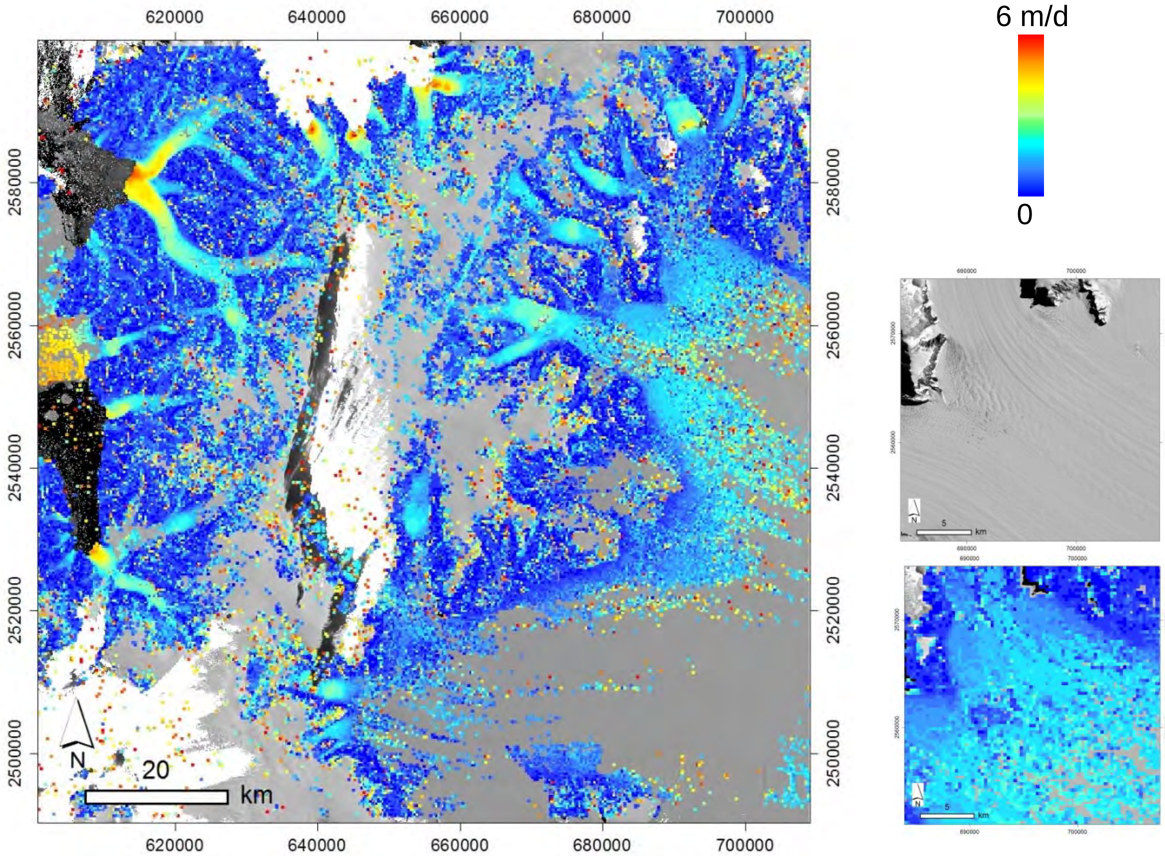

Figure 17. Ice speeds on a section of the Antarctic Peninsula (Larsen C ice shelf to the right) from Sentinel-2 data of 8. and 18. Jan 2016. White areas are clouds in either of the images automatically detected and combined from band 11/band 8 ratios. Displacements with low correlation values (due to clouds, fog, lack of contrast, features larger than matching window used) have been masked out.

5. Conclusions

In this contribution, we analyse the radiometric and geometric performance of Sentinel-2 data with focus on glaciological applications, and evaluate the potential of repeat Sentinel-2 data for measuring glacier flow. Our studies are mainly based on ramp-up phase data, but also on some commissioning phase data.

For dark surfaces, we find along-track stripes of one pixel in width and an amplitude on the order of a few digital numbers, presumably from the precision of destriping/radiometric calibration. Such biases will typically have negligible effect on automated ice/snow mapping. On brighter surfaces only radiometric differences between the 12 pushbroom modules forming the Sentinel-2 focal plane may turn out, with steps of up to a few tens of digital numbers. Also these offsets should typically not affect ice and snow mapping, but might become visible in some segmentation or classification products.

Overall lateral offsets between Sentinel-2 L1C data from repeat orbits are typically on the order of 10 m or below, i.e. equal or smaller than the pixel size of the Sentinel-2 10m bands. These values might improve in the future with co-registration of the data to a reference data set. Within L1C data from repeat orbits, lateral offsets on the order of 1-2 m become in parts visible between the swaths of the individual 12 pushbroom modules.

Importantly, even if the above radiometric and geometric biases might seem unsatisfying for a few high-precision applications, the detectability of these effects in fact proves a very low radiometric and geometric noise level in the Sentinel-2 data analysed. As the effects seen are systematic they can in principle be corrected by the user, or through updates of the processing system or calibration parameters used. Or, simply, it is better to see such effects than have them hidden in noise.

In contrast to the small offsets between repeat-orbit data, lateral offsets between Sentinel-2 data from different orbits, or between Sentinel-2 and other data, such as Landsat, are strongly affected by vertical misrepresentations of the DEM used for orthorectification of the data (and also used for focusing of the different bands and pushbroom modules) that propagate into cross-track offsets. In the worst case, a DEM error of 1 unit leads to a cross-track offset between two scenes of about 1/3 unit. In practice such offsets can amount to several 10-m pixels in size. In relation to existing georeferenced information, these effects become smaller as they do not sum up from two scenes, but may still reach several pixels. The impacts from these propagated DEM errors range from comparably small problems over flat areas within the SRTM DEM cover, to SRTM cover in mountains with typical InSAR problems, and to areas outside the SRTM cover with potentially large DEM errors. In northern Norway for instance, locally varying cross-track offsets of 30-50 m between Sentinel-2 L1C (or Sentinel-2 and Landsat) data from different orbits seem not uncommon, and we expect similar values for other (mountain?) areas outside the SRTM cover.

Such values of > 1 pixel for lateral offsets become actually typical over glaciers, both within and outside SRTM coverage, as DEMs are almost by necessity outdated over glaciers with respect to the date of image acquisition. In the case of SRTM (acquisition in February 2000), > 15 yr of glacier thickness change, mostly loss, come into effect. For reference, glacier elevation losses of 5 m/yr and more are not untypical for glacier tongues in the European Alps [17,33]. As a result, tracking ice velocities between repeat Sentinel-2 data from different orbits, or between Sentinel-2 and Landsat data becomes often problematic for small displacements of a few pixels or less, and should be applied only for ice displacements that are one or several orders of magnitude larger than the cross-track offsets due to DEM errors expected over the glacier studied.

For repeat-orbit Sentinel-2 data, however, we find an impressive potential for ice flow measurements. The good radiometric and geometric performance of Sentinel-2 allows quantification of seasonal ice velocities even over 10-day cycles. We demonstrate this potential for Aletsch Glacier (Swiss Alps), Fox Glacier (New Zealand Alps), Jacobshavn Glacier and neighbouring outlet glaciers of the Western Greenland Icesheet, and a section of the Antarctic Peninsula close to the Larsen C ice shelf. The launch of Sentinel-2B and with that the availability of 5-day repeat orbits will even further increase this potential, at least by reducing the probability of cloud cover. By triangulating displacement measurements between three subsequent acquisitions we show that ice velocities can be measured at least with an accuracy of 1-2 m, i.e. 10-20% of a 10-m pixel. This opens for a number of new possibilities for investigating glacier flow and its spatio-temporal variations, and terrain deformations in general.

Acknowledgments: The study was in parts funded by the European Research Council under the European Union's Seventh Framework Programme (FP/2007–2013)/ERC grant agreement no. 320816, the ESA project Glaciers_cci (4000109873/14/I-NB) and by the Norwegian Space Center contract NIT.06.15.5. We are very grateful to ESA for provision of the Copernicus Sentinel-2 data through the Sentinel Science Hub and Sentinel-2 Expert Users Data Hub, and USGS for provision of the Landsat data through EarthExplorer.

Author Contributions: A.K. designed the study, performed most analyses and wrote the paper. S.W. performed the radiometric analyses, contributed to the other analyses, and wrote the paper. B.A. contributed the orbit calculations and edited the paper. C.N. contributed important discussions and edited the paper. T.N. and J.W. performed the displacement measurements over Greenland and wrote the paper.

Conflicts of Interest: The authors declare no conflict of interest.

Abbreviations

The following abbreviations are used in this manuscript:

DEM: Digital elevation model
DN: Digital number
ETM: Enhanced thematic mapper
MSI: Multispectral instrument
SWIR: Short-wave infrared
OLI: Operational land imager
VNIR: Visible and near infrared

References

1. Paul, F.; Bolch, T.; Kääb, A.; Nagler, T.; Nuth, C.; Scharrer, K.; Shepherd, A.; Strozzi, T.; Ticconi, F.; Bhambri, R., *et al.* The glaciers climate change initiative: Methods for creating glacier area, elevation change and velocity products. *Remote Sens Environ* **2015**, *162*, 408-426.
2. Roy, D.P.; Wulder, M.A.; Loveland, T.R.; Woodcock, C.E.; Allen, R.G.; Anderson, M.C.; Helder, D.; Irons, J.R.; Johnson, D.M.; Kennedy, R., *et al.* Landsat-8: Science and product vision for terrestrial global change research. *Remote Sens Environ* **2014**, *145*, 154-172.
3. Drusch, M.; Del Bello, U.; Carlier, S.; Colin, O.; Fernandez, V.; Gascon, F.; Hoersch, B.; Isola, C.; Laberinti, P.; Martimort, P., *et al.* Sentinel-2: ESA's optical high-resolution mission for GMES operational services. *Remote Sens Environ* **2012**, *120*, 25-36.
4. Gascon, F.; Cadau, E.; Colin, O.; Hoersch, B.; Isola, C.; Fernandeza, B.L.; Martimort, P. Copernicus Sentinel-2 mission: Products, algorithms and cal/val. *Earth Observing Systems Xix* **2014**, *9218*.
5. Winsvold, S.H.; Andreassen, L.M.; Kienholz, C. Glacier area and length changes in Norway from repeat inventories. *Cryosphere* **2014**, *8*, 1885-1903.
6. Paul, F.; Barrand, N.E.; Baumann, S.; Berthier, E.; Bolch, T.; Casey, K.; Frey, H.; Joshi, S.P.; Konovalov, V.; Le Bris, R., *et al.* On the accuracy of glacier outlines derived from remote-sensing data. *Ann Glaciol* **2013**, *54*, 171-182.
7. Winsvold, S.H.; Kääb, A.; Nuth, C. Regional glacier mapping using optical satellite data time series. *Ieee J-Stars* **2016**, 1-14.
8. Kääb, A.; Lamare, M.; Abrams, M. River ice flux and water velocities along a 600 km-long reach of lena river, siberia, from satellite stereo. *Hydrology and Earth System Sciences* **2013**, *17*, 4671-4683.
9. Nuth, C.; Kääb, A. Co-registration and bias corrections of satellite elevation data sets for quantifying glacier thickness change. *Cryosphere* **2011**, *5*, 271-290.
10. Paul, F.; Winsvold, S.H.; Kääb, A.; Nagler, T. Glacier remote sensing using Sentinel-2. Part II: Mapping glacier extents and surface facies, and comparison to Landsat-8. *Remote Sensing* **2016**, submitted.

11. Kääb, A.; Vollmer, M. Surface geometry, thickness changes and flow fields on creeping mountain permafrost: Automatic extraction by digital image analysis. *Permafrost Periglac* **2000**, *11*, 315-326.
12. Heid, T.; Kääb, A. Evaluation of existing image matching methods for deriving glacier surface displacements globally from optical satellite imagery. *Remote Sens Environ* **2012**, *118*, 339-355.
13. Necsoiu, M.; Leprince, S.; Hooper, D.M.; Dinwiddie, C.L.; McGinnis, R.N.; Walter, G.R. Monitoring migration rates of an active subarctic dune field using optical imagery. *Remote Sens Environ* **2009**, *113*, 2441-2447.
14. Hermas, E.; Leprince, S.; Abou El-Magd, I. Retrieving sand dune movements using sub-pixel correlation of multi-temporal optical remote sensing imagery, northwest Sinai peninsula, Egypt. *Remote Sens Environ* **2012**, *121*, 51-60.
15. Pfeffer, W.T.; Arendt, A.A.; Bliss, A.; Bolch, T.; Cogley, J.G.; Gardner, A.S.; Hagen, J.O.; Hock, R.; Kaser, G.; Kienholz, C., *et al.* The Randolph glacier inventory: A globally complete inventory of glaciers. *J Glaciol* **2014**, *60*, 537-552.
16. Howat, I.M.; Negrete, A.; Smith, B.E. The Greenland ice mapping project (GIMP) land classification and surface elevation data sets. *Cryosphere* **2014**, *8*, 1509-1518.
17. Joerg, P.C.; Morsdorf, F.; Zemp, M. Uncertainty assessment of multi-temporal airborne laser scanning data: A case study on an alpine glacier. *Remote Sens Environ* **2012**, *127*, 118-129.
18. Dunse, T.; Schellenberger, T.; Hagen, J.O.; Kääb, A.; Schuler, T.V.; Reijmer, C.H. Glacier-surge mechanisms promoted by a hydro-thermodynamic feedback to summer melt. *Cryosphere* **2015**, *9*, 197-215.
19. Kääb, A.; Huggel, C.; Fischer, L.; Guex, S.; Paul, F.; Roer, I.; Salzmann, N.; Schlaefli, S.; Schmutz, K.; Schneider, D., *et al.* Remote sensing of glacier- and permafrost-related hazards in high mountains: An overview. *Nat Hazard Earth Sys* **2005**, *5*, 527-554.
20. Heid, T.; Kääb, A. Repeat optical satellite images reveal widespread and long term decrease in land-terminating glacier speeds. *The Cryosphere* **2012**, *6*, 467-478.
21. Debella-Gilo, M.; Kääb, A. Sub-pixel precision image matching for measuring surface displacements on mass movements using normalized cross-correlation. *Remote Sens Environ* **2011**, *115*, 130-142.
22. Kääb, A. Correlation image analysis software (cias), http://www.mn.uio.no/icemass.
23. Redpath, T.A.N.; Sirguey, P.; Fitzsimons, S.J.; Kääb, A. Accuracy assessment for mapping glacier flow velocity and detecting flow dynamics from ASTER satellite imagery: Tasman glacier, new zealand. *Remote Sens Environ* **2013**, *133*, 90-101.
24. Ahn, Y.; Howat, I.M. Efficient automated glacier surface velocity measurement from repeat images using multi-image/multichip and null exclusion feature tracking. *Ieee T Geosci Remote* **2011**, *49*, 2838-2846.
25. Schubert, A.; Faes, A.; Kääb, A.; Meier, E. Glacier surface velocity estimation using repeat TerraSAR-x images: Wavelet- vs. correlation-based image matching. *Isprs J Photogramm* **2013**, *82*, 49-62.

26. Prats, P.; Scheiber, R.; Reigber, A.; Andres, C.; Horn, R. Estimation of the surface velocity field of the aletsch glacier using multibaseline airborne sar interferometry. *Ieee T Geosci Remote* **2009**, *47*, 419-430.
27. Wang, D.; Kääb, A. Modeling glacier elevation change from dem time series. *Remote Sensing* **2015**, *7*, 10117-10142.
28. Herman, F.; Anderson, B.; Leprince, S. Mountain glacier velocity variation during a retreat/advance cycle quantified using sub-pixel analysis of ASTER images. *J Glaciol* **2011**, *57*, 197-207.
29. Gjermundsen, E.F.; Mathieu, R.; Kääb, A.; Chinn, T.; Fitzharris, B.; Hagen, J.O. Assessment of multispectral glacier mapping methods and derivation of glacier area changes, 1978-2002, in the central southern alps, New Zealand, from ASTER satellite data, field survey and existing inventory data. *J Glaciol* **2011**, *57*, 667-683.
30. Debella-Gilo, M.; Kääb, A. Measurement of surface displacement and deformation of mass movements using least squares matching of repeat high resolution satellite and aerial images. *Remote Sensing* **2012**, *4*, 43-67.
31. Nagler, T.; Rott, H.; Hetzenecker, M.; Wuite, J.; Potin, P. The Sentinel-1 mission: New opportunities for ice sheet observations. *Remote Sensing* **2015**, *7*, 9371-9389.
32. Haug, T.; Kääb, A.; Skvarca, P. Monitoring ice shelf velocities from repeat MODIS and Landsat data - a method study on the Larsen C ice shelf, Antarctic peninsula, and 10 other ice shelves around Antarctica. *Cryosphere* **2010**, *4*, 161-178.
33. Paul, F.; Haeberli, W. Spatial variability of glacier elevation changes in the Swiss Alps obtained from two digital elevation models. *Geophys Res Lett* **2008**, *35*, L21502.